Impedance spectroscopy of micron sized magnetic tunnel junctions with MgO tunnel barrier

Snorri Ingvarsson,[1,a)] Mustafa Arikan,[1] Matthew Carter,[2] Weifeng Shen,[2] and Gang Xiao[3]

[1]*Science Institute, University of Iceland, Dunhagi 3, Reykjavik IS-107, Iceland*
[2]*Micro Magnetics, Inc., 617 Airport Road, Fall River, Massachusetts 02720, USA*
[3]*Physics Department, Brown University, Providence, Rhode Island 02912, USA*

We have studied the magnetoimpedance of micron sized magnetic tunnel junction sensors with 1.7 nm MgO tunnel barrier. We performed ac impedance spectroscopy in the frequency range between 100 Hz–40 MHz as a function of applied magnetic field in the sensing direction. We model our devices with a simple RLC circuit. Fitting the model to our data results in frequency independent R, L, and C, and our low frequency results are in agreement with dc measurements. Despite excellent agreement with published result on interface capacitance for MgO barrier magnetic tunnel junctions similar to ours we do not observe any magnetocapacitance in our devices. © 2010 American Institute of Physics. [doi:10.1063/1.3449573]

In addition to being ideally suited as nonvolatile magnetic random access memory, magnetic tunnel junctions (MTJs) are excellent magnetic field sensors.[1] As such, they are used in read-write heads in the magnetic storage industry and play a big role in the increase in storage density in the past few years.[2] They have also found applications in magnetic microscopy.[3]

Recently, ac impedance spectroscopy of the MTJs has received considerable interest because the above mentioned applications require high speed functionality and small devices (Al-oxide tunnel barriers,[4–7] MgO tunnel barriers,[8,9] at least one electrode nonmagnetic).[10,11] All of these studies dealt with "large area" devices of ~ 1000 μm^2 or larger. They have exposed a magnetic configuration dependence of the MTJ capacitance, called tunneling magnetocapacitance in analogy with tunneling magnetoresistance (TMR). In this paper we present results of an ac impedance spectroscopy study of individual micron-scale MTJs in the sensor mode, with MgO as the tunnel barrier.

When, in the absence of any external field applied, the magnetic moments of two ferromagnetic electrodes of a tunnel junction are aligned parallel or antiparallel with respect to each other then the MTJ is said to be in the memory (or switching) mode. The resistance-field behavior is hysteretic and switches abruptly between the two extreme resistance states. However, in the sensor mode, the ideal situation is a resistance-field transfer curve that is a one-to-one function with zero coercivity but steep slope dR/dH in the sensing dynamic range. Here R is the junction resistance and H is the applied field. This situation can be achieved, at least approximately, by setting the magnetic moments of the two ferromagnetic electrodes perpendicular to each other. In real devices some hysteresis may remain.

The structure of the devices used in this work is as follows (thicknesses in nanometers): Ta(5)/ Ru(30)/Ta(5)/$Co_{50}Fe_{50}$(2)/IrMn(15)/$Co_{50}Fe_{50}$(2)/Ru(0.8)/ $Co_{40}Fe_{40}B_{20}$(3)/MgO(1.7)/$Co_{40}Fe_{40}B_{20}$(3)/Ta(5)/Ru(10). They were sputter deposited on thermally oxidized Si wafer substrates. An artificial antiferromagnetic CoFe/Ru/CoFeB

trilayer structure has been used for the purpose of increasing exchange bias and for thermal stability enhancement. It is also important for preventing Mn diffusion from the IrMn layer into the MgO tunnel barrier at high temperatures. Details regarding sample fabrication and optimization are reported elsewhere.[12] The junctions were patterned into ellipses with major and minor axes of 2 μm and 4 μm, respectively. Postdeposition thermal annealing was performed in high vacuum at a temperature of 310 °C for 1 h with an applied field of 4.5 kOe. To set the junctions in the sensor configuration, the pinned layer magnetization is set perpendicular to the free layer's easy axis.

Our setup included an electromagnet capable of producing up to ±90 Oe dc-field. Electrical measurements were performed using a Keithley 2400 source-meter for dc-TMR (with about 100 mV applied voltage) and a HP 4194A impedance analyzer (100 Hz to 40 MHz) for ac impedance spectroscopy with an HP 16085B measurement fixture (4-probe technique, 100 mV ac voltage). We used standard calibration methods (open, short, and load) before each measurement to cancel the effects of cables and leads. Several complex RLC circuits were constructed and measured by
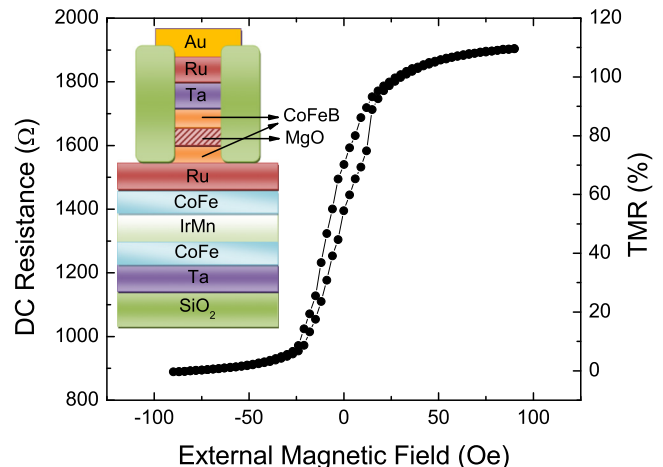

FIG. 1. (Color online) dc magnetoresistance curve for MTJ-1. Inset: device structure.

TABLE I. dc-resistance measurements.

MTJ	R_{ap} (Ω)	R_p (Ω)	TMR (%)	Coercivity (Oe)
1	1980	890	132	3
2	2420	1020	137	2
3	2100	965	118	2

TABLE II. Model parameters extracted from data, based on Eqs. (1) and (2).

MTJ	R_{ap} (Ω)	R_p (Ω)	C_{ap} (pF)	C_p (pF)	L_{ap} (μH)	L_p (μH)
1	1905	890	6.5	6.5	0.28	0.28
2	2385	1095	7.5	7.5	0.35	0.35
3	2050	977	7.5	7.5	0.25	0.25

using standard circuit components in order to find out our measurement sensitivity, in particular to small capacitances, as our devices are small. We were able to measure capacitance values down to 0.06 pF quite reliably in configurations mimicking our MTJ devices.

Here we present results for three nominally identical devices (MTJ-1, 2, and 3). The dc-TMR curve for MTJ-1 is given in Fig. 1. It shows that the tunnel junction is in the sensing mode with a small coercivity of 3 Oe. The sensor has a field dynamic range of ±20 Oe. Similar results were obtained for the junctions MTJ-2 and MTJ-3. These are detailed in Table I. Our TMR value is defined as the by now conventional $100 \times (R_{ap}-R_p)/R_p$, where $R_{ap}(R_p)$ is the resistance with antiparallel (parallel) configuration of the magnetic electrodes. The total MR for the three samples is in the range of 118%–137%.

Figure 2 displays the frequency dependence of the real and imaginary parts of the impedance, in parallel (−90 Oe) and antiparallel (+90 Oe) states for MTJ-1. Also shown, are results in zero field, with the free and pinned layer magnetization mutually perpendicular. Similar behavior was observed for MTJ-2 and MTJ-3. A priori, one expects the MTJ sensor to behave like a "leaky capacitor," the leakiness stems from the tunnel current. Thus it should be representable by a parallel RC circuit. This assumption is supported by our results, which show a characteristic dip for an RC circuit as seen in Fig. 2. [The RC cut-off frequency increases as the junction is swept from high resistance (9 MHz) to low resistance state (20 MHz)]. Also the Cole–Cole diagrams show circular patterns that suggests that the circuit model should have parallel RC networks. Our goal was to work with the simplest possible model that would fit our data. However, it

turned out that the simple model of one resistor in parallel with a capacitor does not quite capture all the details of our data for any of the three junctions we report here. The reason is due to the short section of wire bonds and on-chip wiring leading up to the MTJ that we did not compensate for in our calibration. This wiring contributes an inductive component in series with the simple RC circuit described above (see Fig. 2 inset). The complex impedance, $Z = \text{Re}(Z) + i \, \text{Im}(Z)$, for this circuit model can be written as,

$$\text{Re}(Z) = \frac{R}{1 + (\omega RC)^2}, \tag{1}$$

$$\text{Im}(Z) = \omega L - \frac{\omega R^2 C}{1 + (\omega RC)^2}. \tag{2}$$

For an unknown MTJ this presents two equations for three unknowns, namely, R, L, and C. However, R can be obtained from the low frequency limit (and it should, and does, agree with the dc measurements). Then L and C can be determined readily by fitting Eqs. (1) and (2) to the data. Using this model we were able to fit our data with *fixed* values of L and C, and two values for R that correspond to parallel and antiparallel alignment, respectively. All the parameters are frequency independent, as one hopes to find if such a lumped circuit element model is to faithfully represent the physical system. Results of our fits to all three devices are detailed in Table II.

Our data can be fit by more complex models but in these cases we find there are simply too many fit parameters, some of which usually end up with unreasonable or unphysical numerical values. It is worth emphasizing that our results show no dependence of the capacitance on relative magnetization orientation of the ferromagnetic electrodes, i.e., we see *no* hint of a magnetocapacitance effect. This appears to be in contradiction with careful studies that have demonstrated the existence of such an effect,[6,8,10] explained theoretically in Refs. 13 and 14. However, it is important to realize that our measured capacitance is a combination of different contributions. Taken at face value our capacitance results yield an effective dielectric constant for the MgO insulator that is much larger than the bulk value of $\epsilon = 9.7\epsilon_0$. This has been explained previously by an interface capacitance C_i, in series with the geometric capacitance $C_g = \epsilon A/d$ of the insulating MgO layer, where A is the junction area, and d is the MgO thickness.[4,8,10] The measured capacitance is thus

$$\frac{1}{C} = \frac{1}{C_g} + \frac{1}{C_i}. \tag{3}$$

This interface capacitance can include contribution from surface roughness, interface states (in which case one would see a frequency dependence of our model parameters),[11] and charge accumulation and screening at the metal/insulator
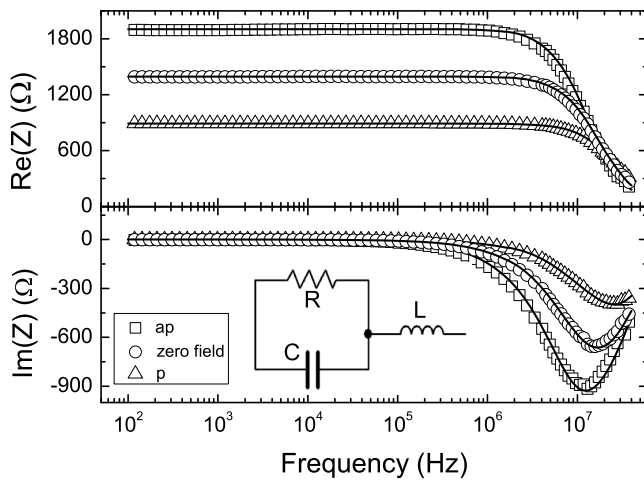

FIG. 2. Real and imaginary impedance as a function of frequency at room temperature for the parallel and antiparallel magnetization configurations, as well as for the zero field perpendicular (sensing) magnetization orientation. The solid lines are the fit to the data by using the equivalent circuit (inset) as explained in the text. For clarity we have reduced the number of data points.

interfaces.[15] The last mentioned contribution is observed in normal metal capacitors[11] but develops another level of complexity when the electrodes are ferromagnetic, as the exchange interaction causes a spin dependent screening potential.[14] This is what causes the above mentioned magnetocapacitance effect.[13]

Upon inserting $C_g = 0.317$ pF for our 6.28 μm^2 device into Eq. (3) with $C = 6.5$ pF, we obtain $C_i = -0.334$ pF. The negative value of C_i is associated with a negative screening length and oscillatory screening that results in excess pile-up of screening charge on the interface charges, as explained by Miesenböck and Tosi.[16] Our results correspond to $C_i/A = -5.31$ $\mu F/cm^2$, i.e., -10.62 $\mu F/cm^2$ per interface. This agrees quite well with the results in Ref. 8, where they report -12.8 $\mu F/cm^2$ and -13.2 $\mu F/cm^2$, respectively, for the parallel and antiparallel configurations.

How can magnetocapacitance be completely absent in our results, while both Padhan *et al.*[8] and Kaiju *et al.*[6] observe such an effect, of up to 50%? We apply the same model to fit our data and obtain very similar results for C_i. The main difference in our studies lies in the sample size ($\gtrsim 1000$ μm^2 or larger versus ~ 1 μm^2 in our samples) and the relative orientation of the magnetic electrodes at zero applied field (memory versus sensor configuration). Assuming the edge lengths of our junctions are much larger than the characteristic wavelength for surface roughness[17] and that we can neglect contribution from surface states then C_i scales with area much like the geometric capacitance C_g. By that argument the area of the sample should not affect the visibility of any magnetocapacitance effect. Also, whether samples are set in memory or sensor configurations should have no effect, as it is well known that the last monolayer or two at the interface dictate the spin of the tunneling electrons. At this point we cannot completely rule out the possibility of a fringe capacitance that is independent of magnetization and becomes dominant in smaller samples because it scales with the perimeter length, as opposed to the area. It is difficult to see how we could get such good agreement for the interface capacitance in that case. A systematic study of different sized MTJs would resolve this specific issue.

In summary, we have fabricated micron scale MTJ sensors with MgO tunnel barrier and characterized them by using complex impedance spectroscopy. We obtain high TMR ratios in the range of 118%–137%. However, in contrast with two previous studies in the literature, we observed no sign of a magnetocapacitance effect. We can only speculate about the reason for this, the only obvious difference of possible significance between our study and previous ones is the sample size. The effects of electron-electron interaction and spin dependent screening (resulting in interface capacitance) on the frequency dependence MTJs are rather poorly understood and deserve more study both from experimental and theoretical vantage points.

[1] D. Mazumdar, W. Shen, X. Liu, B. Schrag, M. Carter, and G. Xiao, J. Appl. Phys. **103**, 113911 (2008).

[2] C. Chappert, A. Fert, and F. N. V. Dau, Nature Mater. **6**, 813 (2007).

[3] W. Shen, X. Liu, D. Mazumdar, and G. Xiao, Appl. Phys. Lett. **86**, 253901 (2005).

[4] G. Landry, Y. Dong, J. Du, X. Xiang, and J. Xiao, Appl. Phys. Lett. **78**, 501 (2001).

[5] M. Gillies, A. Kuiper, R. Coehoorn, and J. Donkers, J. Appl. Phys. **88**, 429 (2000).

[6] H. Kaiju, S. Fujita, T. Morozumi, and K. Shiiki, J. Appl. Phys. **91**, 7430 (2002).

[7] W. Chien, C. Lo, L. Hsieh, Y. Yao, X. Han, Z. Zeng, T. Peng, and P. Lin, Appl. Phys. Lett. **89**, 202515 (2006).

[8] P. Padhan, P. LeClair, A. Gupta, K. Tsunekawa, and D. Djayaprawira, Appl. Phys. Lett. **90**, 142105 (2007).

[9] J. Huang, C. Hsu, W. Chen, and Y. Lee, IEEE Trans. Magn. **43**, 911 (2007).

[10] K. McCarthy, A. Hebard, and S. Arnason, Phys. Rev. Lett. **90**, 117201 (2003).

[11] K. McCarthy, S. Arnason, and A. Hebard, Appl. Phys. Lett. **74**, 302 (1999).

[12] X. Liu, D. Mazumdar, W. Shen, B. Schrag, and G. Xiao, Appl. Phys. Lett. **89**, 023504 (2006).

[13] S. Chui and L. Hu, Appl. Phys. Lett. **80**, 273 (2002).

[14] S. Zhang, Phys. Rev. Lett. **83**, 640 (1999).

[15] D. Newns, Phys. Rev. B **1**, 3304 (1970).

[16] H. Miesenböck and M. Tosi, Z. Phys. B: Condens. Matter **78**, 255 (1990).

[17] B. Schrag, A. Anguelouch, S. Ingvarsson, and G. Xiao, Appl. Phys. Lett. **77**, 2373 (2000).